Journal of Materials Chemistry C

ROYAL SOCIETY OF CHEMISTRY

PAPER

View Article Online
View Journal | View Issue

Cite this: J. Mater. Chem. C, 2025, 13, 7625

Photoluminescence enhancement of quasi-2D perovskite films by plasmonic silver nanoparticles†

Emmanuel delaCruz-Pina,[ab] Carina Pareja-Rivera,[cd] Dulce Zugasti-Fernandez,[c] Arturo Rodriguez-Gomez,[a] Diego Solis-Ibarra *[c] and Jorge Alejandro Reyes-Esqueda *[ae]

Received 8th October 2024,
Accepted 3rd March 2025

DOI: 10.1039/d4tc04288c

rsc.li/materials-c

Metal halide perovskites have emerged as leading materials in luminescence and photovoltaic research due to their unique tunable optical properties, with applications spanning light sources, sensors and solar cells. Recently, quasi-2D perovskites, characterized by their enhanced stability and superior moisture resistance, have gained attention for their potential in ambient-condition applications. Enhancing the properties of these materials to enable the development of highly efficient devices that can operate under ambient conditions has become a critical and highly active area of research. This study investigates the photoluminescence (PL) enhancement of $(PEA)_2(MA)_{n-1}Pb_nI_{3n+1}$ perovskite films, with n = 3, 5, 10, through the deposition of silver nanoparticles (Ag NPs) *via* sputtering. The size distribution and absorbance spectrum of Ag NPs were systematically analyzed to identify conditions for maximum PL amplification. The results show that the strongest PL enhancement, a 7.4-fold increase, was achieved for n = 10 films coated with Ag NPs exhibiting a plasmonic resonance peak at 528 nm and a size distribution peak at 8 nm. This study provides critical insights into the interaction between plasmonic nanostructures and quasi-2D perovskites, preparing the path for the development of highly stable and highly efficient light-emitting devices and solar cells.

1. Introduction

Perovskites are among the most innovative materials in the research of luminescence and photovoltaic processes.[1–4] In particular, metal halide perovskites have been the new bases for the fabrication of nanolasers,[5] photovoltaic solar cells,[6] and quantum light sources.[7] The general formula of 3D perovskites is ABX_3, where A is a monovalent cation, B is a metal such as Pb^{2+}, Sn^{2+}, and X corresponds to a halide such as Cl, Br, I. The cation A typically is Cs^+, $CH_3NH_3^+$ (methylammonium or MA) or $CH_5N_2^+$ (formamidinium or FA).[6–10] The diverse combinations of cations (A and B) and, notably, the mixtures of different anions (X) enable perovskites to achieve tunable bandgaps, ranging from 1.2 to 3 eV, with well-defined emission between 400 and 1000 nm wavelengths.[5]

Furthermore, it is possible to add a fourth component (A′) to separate sections of the perovskite and create quasi-2D perovskite sheets increasing chemical and thermal stability, as organic layers act as barriers against water and external agents.[11] The general formula for this family of perovskites is $(A')_mA_{n-1}B_nX_{3n+1}$, where A′ is a cation that intercalates between perovskite layers, with m = 2 for monovalent cations and m = 1 for divalent cations, and n the number of interconnected octahedral layers. For lead halide perovskites, only a small number of organic or inorganic A-cations present stable 3D phases (like MA, FA, or Cs), and the most commonly used A′-cation spacers are phenethylammonium (PEA), butylammonium (BA) or octylammonium (OA).[12] These additional cations, with their moderated size, provide stability while preserving the integrity of the structure. In particular, $(PEA)_2(MA)_{n-1}Pb_nI_{3n+1}$ has proven ideal for applications under ambient conditions. $(PEA)_2(MA)_2Pb_3I_{10}$ (n = 3) perovskite films have shown impressive tolerance and stability, particularly concerning moisture stability, under ambient-like conditions.[13] These advanced materials feature a wider bandgap (>2.0 eV) due to quantum confinement, more intense photoluminescence emission ideal

[a] Instituto de Física, Universidad Nacional Autónoma de México. Circuito de la Investigación Científica, Ciudad Universitaria, Coyoacán, 04510, Mexico City, Mexico. E-mail: reyes@fisica.unam.mx
[b] Engineering and Technology Institute Groningen (ENTEG), Faculty of Science and Engineering, University of Groningen, 9747 AG, Groningen, The Netherlands
[c] Laboratorio de Fisicoquímica y Reactividad de Superficies (LaFReS), Instituto de Investigaciones en Materiales, Universidad Autónoma de México UNAM, Coyoacán, 04510, Ciudad de México, Mexico. E-mail: diego.solis@unam.mx
[d] Institute of Advanced Materials (INAM), Universitat Jaume I. Avenida de Vicent Sos Baynat, s/n. Castelló de la Plana, Castellón, Spain
[e] Département de Physique, Faculté des Sciences, Université de Sherbrooke, J1K 2R1, Sherbrooke, QC, Canada

† Electronic supplementary information (ESI) available: Sputtering process for Ag NP coatings, PL intensity measurements of perovskite films, and TEM images with size distributions of Ag NPs. See DOI: https://doi.org/10.1039/d4tc04288c

for LEDs and lasers, and more stable excitons with high binding energy (~100–300 meV) from layer confinement.

On the other hand, plasmonic nanostructures play an important role in the development of highly efficient light-emitting devices, highly sensitive sensors, enhancement of quantum emitters, and information transfer, owing to their ability to confine light to nanometric dimensions and create very intense local electromagnetic fields.[14–18] In recent years, the enhancement of the optical properties of materials by plasmonic nanostructures has led to the fabrication of highly efficient nanolasers,[14,19] improved solar cells,[20,21] highly sensitive sensors,[17,22] low-loss waveguides,[15] plasmonic-enhanced light-emitting diodes,[23] and enhanced quantum emitters.[16,24] The basis of these improvements lies in the effects generated by the coupling between the materials and plasmonic nanostructures, such as PL enhancement. This enhancement can be achieved through the direct interaction of photoluminescent materials with metallic NPs.[25–27] Localized surface plasmons (LSP) generated by oscillating electrons in metallic NPs can be induced by either photoluminescence (PL) from an excited material or by an excitation source. Electrons constituting the plasmon are injected into the luminescent material and function as hot carriers within the conduction bands.[25,27–29] Subsequently, they transition to the valence band *via* radiative decay. The resonance wavelength and intensity of the LSP depend on the shape, size, and composition of the metallic NPs, as well as on the properties of the surrounding media.[21,30] On the other hand, incorporating metallic NPs with plasmonic characteristics has proven to be a fruitful strategy for enhancing the performance of solar cells.[31,32] The non-absorbed spectrum from a tandem photovoltaic cell can be used to generate plasmons in metallic nanostructures, whose hot electrons can be transferred to the cell's active medium, increasing in power conversion efficiency (PCE). It has been reported that incorporating Au@TiO_2 NPs in direct contact with or embedded in an active medium composed of $CH_3NH_3PbI_3$ perovskite in a photovoltaic cell can increase its PCE from 12.6% to 18.2%.[33] However, the most suitable characteristics of plasmonic nanostructures for obtaining maximum enhancement of quasi-2D perovskite films are still not fully understood. As many novel lead halide perovskites have emerged, it is highly desirable to understand the influence of different metallic nanostructures on the quasi-2D perovskite optical properties.

In this study, the PL enhancement of $(PEA)_2(MA)_{n-1}Pb_nI_{3n+1}$ (with n = 5, 10) perovskite films were achieved by sputtering of Ag NPs coatings onto the films. The absorbance spectrum and size distribution of the Ag NPs and the PL intensity of the films were analyzed to determine the optimal characteristics of Ag NPs for PL enhancement. PL amplification was observed for various Ag NP depositions and perovskite phases (n = 5, 10). The maximum PL enhancement occurred when the plasmonic resonance wavelength of the Ag NPs matched the 532 nm excitation laser source. A maximum 7.4-fold amplification in the PL intensity was observed for $(PEA)_2(MA)_9Pb_{10}I_{31}$ (n = 10) perovskite films coated with an Ag NPs exhibiting a peak absorbance at 528 nm and NPs size distribution peak at 8 nm.

2. Materials and methods

2.1. Quasi-2D perovskite films synthesis

2.1.1. Materials. Phenethylammonium iodide salt (99%), PbI_2 (99.9%), hydriodic acid (57%), chlorobenzene anhydrous (99.8%), *N*,*N*-dimethylformamide (DMF), and diethyl ether were purchased from Sigma-Aldrich. Isopropanol was purchased from Tecsiquim. Methylamine, 40% w/w aq. This solution was purchased from Alfa Aesar. All the chemicals were used directly without further purification. The solvents used were of reagent grade or higher purity. The DMF and diethyl ether were dried and degassed using a JC Meyer solvent purification system.

2.1.2. Methylammonium iodide. Methylammonium iodide (MAI) was synthesized by mixing concentrated hydroiodic acid (HI, 15.0 mL, 57 wt% in water) with an aqueous methylamine (CH_3NH_2) solution (13.5 mL, 40 wt%) at 0 °C for 2 h under vigorous stirring in a nitrogen atmosphere. Subsequently, all volatiles were removed using a rotary evaporator, and the resulting off-white powder was washed three times with diethyl ether (10 mL) and dried under vacuum overnight. The final product, MAI, was obtained as a white crystalline solid (19.38 g, 78% yield).

2.1.3. Dissolution of $PEA_2MA_{n-1}Pb_nI_{3n+1}$. A 1.0 M solution of $PEA_2MA_{n-1}Pb_nI_{3n+1}$, relative to lead content, was prepared. The reagents were weighed inside a glove box and dissolved in a 4 : 1 DMF : DMSO ratio. The solution was stirred at 70 °C overnight. Before deposition, it was filtered using a 0.22 μm polytetrafluoroethylene (PTFE) membrane.

2.1.4. Glass substrates cleaning. Glass substrates were cleaned before film deposition. First, they were sonicated for 10 min in a mixture of distilled water and Hellmanex III detergent. The substrates were then rinsed twice with hot distilled water and isopropyl alcohol. After each bath, pressurized nitrogen (N_2) was used to dry the samples. Finally, the substrates were treated in a UV-ozone cleaner (Ossila) for 20 min.

The deposition of $(PEA)_2(MA)_{n-1}Pb_nI_{3n+1}$ films (n = 3, 5, and 10) was carried out using a two-step static spin-coating method. First, glass substrates were preheated on a hotplate at 80 °C for 10 min. In the first step, 100 μL of the perovskite precursor solution was dispensed onto the substrate and spun at 1000 rpm for 10 s. In the second step, 200 μL of chlorobenzene was added as an antisolvent during spinning at 3000 rpm for 30 s. Finally, the samples were annealed at 80 °C for 10 minutes and stored in a nitrogen-filled glove box.

2.2. Perovskite optical characterization

The $(PEA)_2(MA)_{n-1}Pb_nI_{3n+1}$ perovskite films displayed optical characteristics according to the sheet thickness. n = 3 phase perovskite films showed peak absorbance at 505 nm wavelength, while n = 5 and n = 10 phase perovskites presented peak absorbance at 563 nm (Fig. 1a). These differences in the absorption spectra are associated with the variations in the bandgaps of the different perovskite phases n.[11] It is important to note that, for the three cases, there is a large absorption at

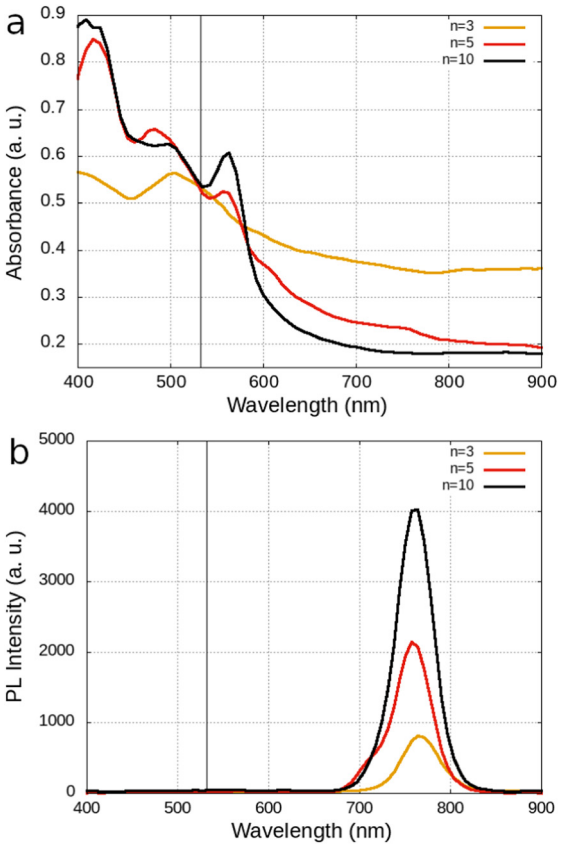

Fig. 1 Optical characteristics of $(PEA)_2(MA)_{n-1}Pb_nI_{3n+1}$. (a) Absorbance spectra for perovskite films with phases n = 3, 5, 10. (b) Photoluminescence spectra corresponding to the same phases.

532 nm, allowing easy excitation of the material at this wavelength. However, it can be noted that the bandgap for the phase n = 3 is significantly larger than for the other phases, and its energy is higher than that of the excitation laser.

The perovskite films were excited using a 532 nm wavelength laser with a power of 1 mW, resulting in distinct PL spectra for each phase n (Fig. 1b). Perovskite films with n = 3 phase exhibited a PL maximum at 764 nm wavelength, along with a considerably lower PL intensity than other types of samples. Conversely, perovskite samples with n = 5 and n = 10 displayed high PL intensity, with PL maxima at 759 nm and 761 nm wavelengths, respectively. Notably, the samples with n = 10 exhibited twice the PL intensities of those with phase n = 5.

2.3. Sputtering coating of Ag NPs

The Ag NPs coatings were generated using a CY-MSP180G-DC sputtering system with an Ag target (99.9%) at a high chamber pressure of 2.5 Pa, deposition time of 1 s, and sputtering surface heating of 75 °C. Deposition time plays a crucial role in the production of NPs under high-pressure conditions within the chamber. Subtle variations in the deposition time and pressure within the sputtering chamber resulted in nuanced alterations in the morphology and size of the Ag NPs (see Section S1, ESI†). Ag coatings exceeding a deposition time of 1 s resulted in porous film layers owing to NP agglomeration. In contrast, deposits lasting only a fraction of a second resulted in deposits containing minimal NPs. The size distribution and absorbance spectrum of the Ag NPs were tuned by varying the sputtering power. Ag NPs were simultaneously deposited on glass substrates and TEM grids for characterization, size distribution analysis, and absorbance spectrum analysis.

The characteristics of Ag NPs were tuned by controlling the plasma power (see Fig. 2). A low sputtering power of 55 W produced small Ag NPs with a size distribution centered at 3 nm and a localized plasmon resonance at a wavelength of

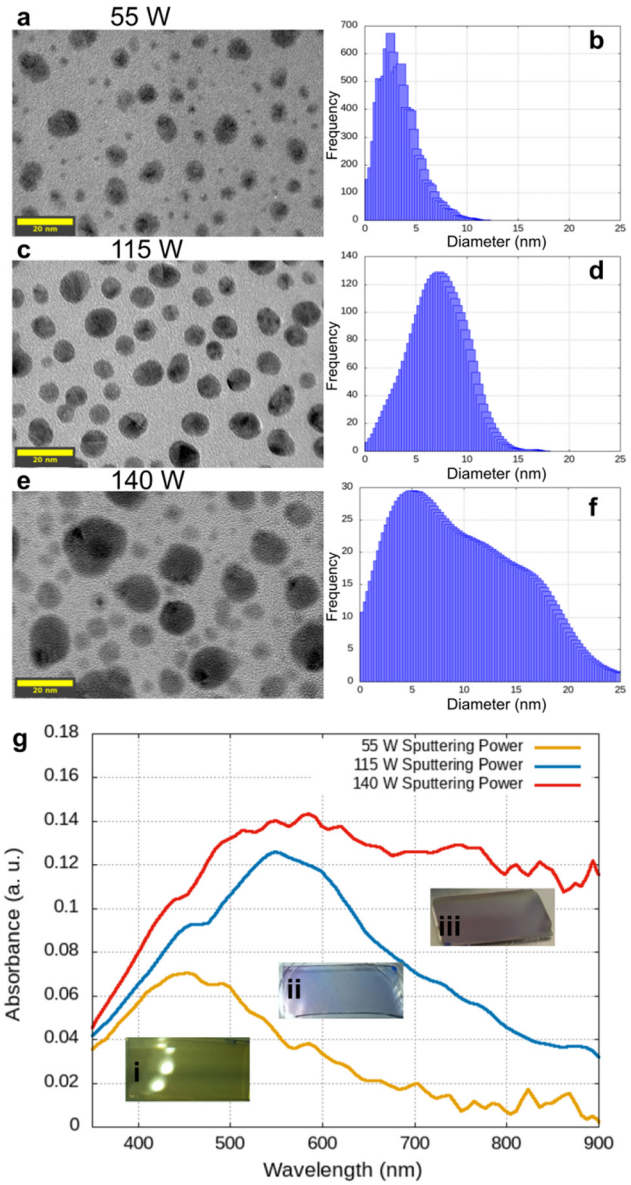

Fig. 2 Sputtered Ag NPs on glass substrates. (a), (c) and (e) TEM images of Ag NPs fabricated at sputtering powers of 55 W, 115 W, and 140 W, respectively (scale bar: 20 nm). (b), (d) and (f) Corresponding size distributions for each sputtering power. (g) Absorbance spectra of Ag NPs deposited at 55 W, 115 W, and 140 W. (i), (ii) and (iii) Insets show images of Ag NPs on glass for sputtering powers.

470 nm (Fig. 2a, b and g). As the sputtering power increased, the size of the Ag NPs grew, accompanied by a red shift in the absorbance spectrum. At a moderate power of 115 W, a well-defined size distribution, shape, and absorbance spectrum were achieved, with a size distribution centered at approximately 8 nm and an absorbance peak between 520 nm and 560 nm (Fig. 2c, d and g). However, when the power exceeded 120 W, deformation and agglomeration of the Ag NPs deposits were observed, along with the disappearance of a distinguishable peak in the absorbance spectra. (Fig. 2e–g). As explained later, deposits with well-defined absorbance peaks, devoid of agglomeration and spherical shapes, are crucial for generating of plasmonic resonance and enhancing PL intensity. The sputtering coatings were deposited simultaneously onto both glass substrates and perovskite films. This approach allowed for the correlation between the absorbance spectrum of the Ag NPs coating and the optical effects observed in the PL spectra of the perovskite films.

3. Results and discussion

Ag NPs coatings were applied onto perovskite films to observe the perovskite PL intensity changes when exposed to a direct lasing source of 532 nm wavelength after the coatings, as shown in Fig. 3. The coatings were also applied simultaneously on glass substrates to measure the absorption spectrum of the Ag NPs and correlate it to the PL changes. An initial trial result of the PL enhancement is shown in Fig. 3c, where the PL of a $(PEA)_2(MA)_9Pb_{10}I_{31}$ (n = 10) perovskite film without (black) and with (purple) the Ag NPs deposit is shown. The PL intensity in the area without Ag NPs (indicated by a green arrow in Fig. 3d) was the same after sputtering coating. Meanwhile, the rest of the films areas showed strong PL enhancement associated with the Ag NPs coating (see Section S2 from ESI†).

Initially, $(PEA)_2(MA)_2Pb_3I_{10}$ (n = 3) perovskite films and glass substrates were coated with different Ag NPs deposits. The Ag NPs deposited on glass presented absorbance peaks ranging from 455 nm to 590 nm (see Fig. 4a). All coatings generated a reduction in the PL intensity of the perovskite films. A coating with a peak absorbance at 455 nm, corresponding to a sputtering power of 47 W, reduced the PL intensity by 0.8-fold. In contrast, a coating with a peak absorbance at 505 nm, generated using a sputtering power of 111 W, quenched the PL intensity by a factor of 0.5. The quenching of the PL is related to the absorbance of the Ag NPs at the excitation wavelength, and to the absorbance of the PL wavelength without plasmonic layer, respectively. This effect is likely also influenced by the intrinsic absorption characteristics of the Ag NPs.

Ag NPs coatings were also applied to $(PEA)_2(MA)_4Pb_5I_{16}$ (n = 5) perovskite films at different power levels (Fig. 5). When the deposition on the glass substrate exhibited an absorbance peak at 470 nm, and a lower absorption near the excitation laser wavelength of 532 nm, the PL intensity remained consistent. However, a notable increase in the intensity was observed for deposits with absorbance peaks close to 532 nm. The deposit

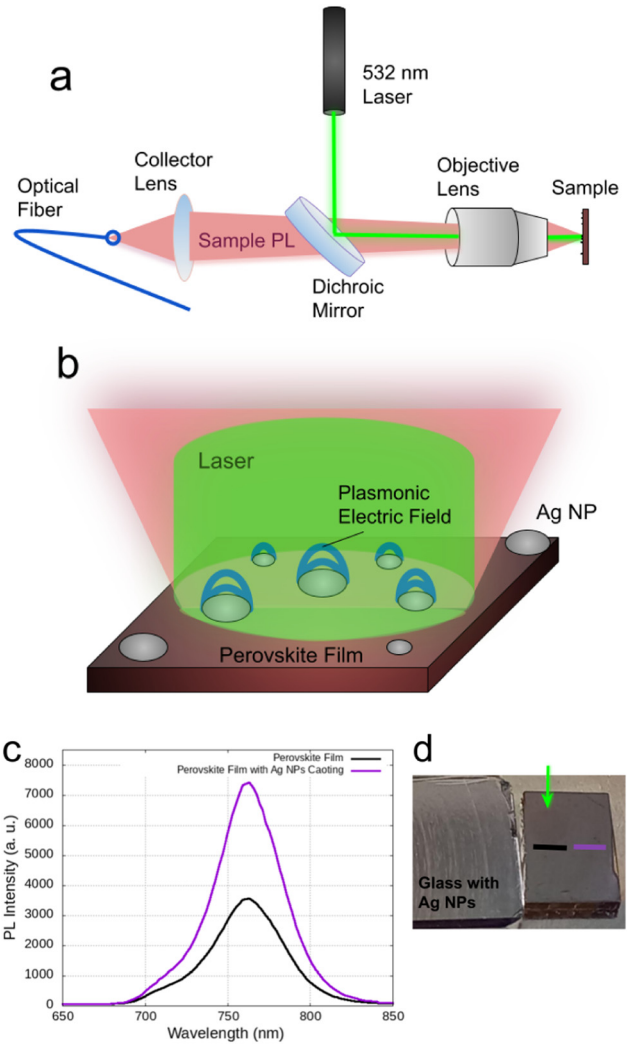

Fig. 3 (a) Optical setup for PL measurements. (b) Schematic representation of the interaction between plasmonic nanoparticles and a perovskite film, where the LSP generates an electric field, leading to increased exciton generation and, consequently, higher PL intensity. (c) Comparison of PL intensity for a $(PEA)_2(MA)_9Pb_{10}I_{31}$ (n = 10) perovskite film with (purple) and without (black) an Ag NPs coating. (d) Glass substrate with an Ag NP coating and a perovskite film, indicating regions without Ag NPs (black line) and with Ag NPs (purple line).

with the highest power, 140 W, achieved maximum absorbance at approximately 532 nm, resulting in a 2-fold increase in the PL intensity. Notably, the most substantial PL enhancement occurred with a power deposit of 115 W and an absorption peak of the deposit on the glass at 530 nm, yielding a 3.7-fold increase in PL intensity.

As shown in Fig. 5, perovskite films with n = 5 exhibited the most significant enhancement when coated with Ag NPs deposited using a sputtering power of 115 W, and when the excitation laser wavelength closely matched the absorbance peak. Under these conditions, the laser beam achieved the highest plasmonic resonance, resulting in a more direct charge injection from the Ag NPs in the perovskite. Although the absorbance peak for the 140 W deposit was higher at 532 nm, the maximum

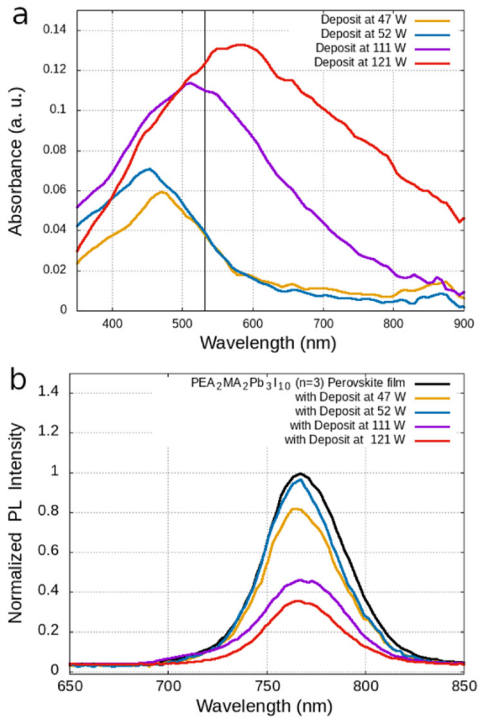

Fig. 4 PL intensity enhancement in perovskite films for n = 3. (a) Absorbance spectra of Ag NPs deposited on glass substrate at different sputtering powers (vertical black line at 532 nm). (b) Normalized PL intensity of the perovskite films without Ag NPs (black line) and with a Ag deposited at sputtering powers of 47 W, 52 W, 111 W, and 121 W.

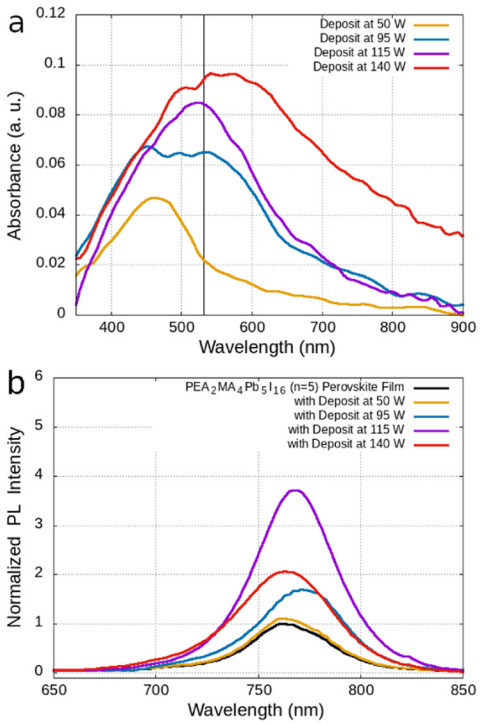

Fig. 5 PL intensity enhancement in perovskite films for n = 5. (a) Absorbance spectra of Ag NPs deposited on glass substrate at different sputtering powers (vertical black line at 532 nm). (b) Normalized PL intensity of the perovskite films without Ag NPs (black line) and with a Ag deposited at sputtering powers of 50 W, 95 W, 115 W, and 140 W.

plasmonic resonance occurred at a longer wavelength. This mismatch reduced the plasmonic intensity when excited by the laser, leading to a lower number of oscillating free charges injected into the film and, consequently, a reduction in the amplification of the PL intensity.

Similarly, coatings of Ag NPs were fabricated at different powers on $(PEA)_2(MA)_9Pb_{10}I_{31}$ (n = 10) perovskite films. A coating deposited at 55 W exhibited an absorbance peak at 440 nm and a minimum absorbance 0.02 at 532 nm (see Fig. 6a). This behavior was attributed to the small size of the Ag NPs generated under these conditions (see Fig. S6, Section S3, ESI†). This deposit resulted in an up to 2-fold increase in PL intensity when the sample was excited with the 532 nm laser beam. A deposit generated at 55 W on the perovskite film produced a maximum absorbance at 450 nm and an absorbance of 0.06 at 532 nm. This deposit led to a more than 3-fold enhancement in PL intensity under laser beam.

A coating deposited at 110 W generated Ag NPs with a maximum absorbance at 495 nm and a high absorbance of 0.12 at 532 nm. This deposit resulted in 4.8-fold increase in PL intensity compared to the uncoated film. The most notable enhancement was achieved in a sample with n = 10, and a deposit generated at 120 W sputtering power. This deposit produced Ag NPs with a peak absorbance at 550 nm, leading to a remarkable 7.4-fold amplification in PL intensity when excited with a 532 nm beam.

Different enhancements in PL intensity were observed across different perovskite phases (n) (Fig. 4–6). Fig. 7 shows the PL amplification of the perovskite films with phases n = 5 and 10 as a function of the characteristics of the Ag NPs deposits. These results suggest that the optimal sputtering power for depositing Ag NPs to enhance the PL of perovskites lies near 115 W. For phase n = 5, the most significant enhancement was observed at a sputtering power of 115 W. In contrast, for phase n = 10, the maximum PL amplification occurred at a sputtering power of 120 W. Another key characteristic of the optimal deposits was their peak and high absorbance near 532 nm, the excitation laser wavelength, which caused variations in plasmonic excitation. The maximum enhancement measured for phase n = 5 was a 3.7-fold increase with an Ag NPs deposit exhibiting an absorbance peak was measured at 528 nm. For phase n = 10, a maximum PL amplification of 7.4-fold was achieved with a deposit having a peak absorbance at 545 nm. These findings indicate that plasmonic resonance and PL amplification were maximized under these deposition conditions.

An important aspect to emphasize is the distinction in the PL amplification generated by Ag NP deposits fabricated at 110 W and 120 W sputtering powers, as shown in Fig. 8. Despite the similarity in their absorbance spectra, significant differences in PL amplification were observed. These differences are attributed to the distinct morphologies of the Ag NPs formed under these conditions (see Fig. S6, Section S3, ESI†). Specifically, deposition at produced Ag NPs with a mixture of spherical and ellipsoidal shapes, while deposition at 110 W resulted in a

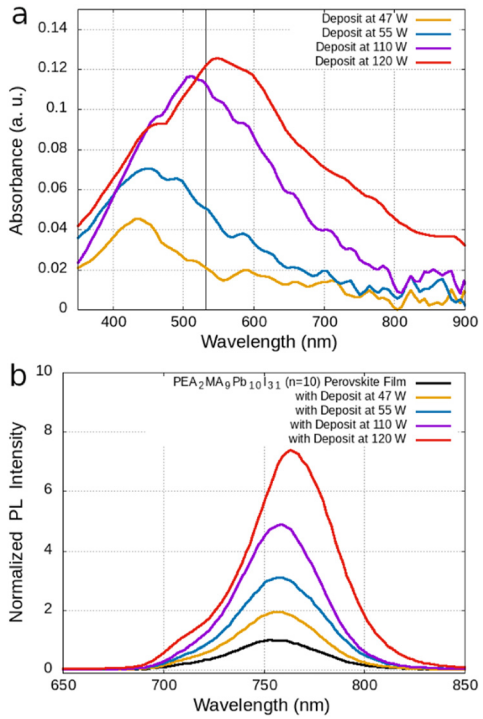

Fig. 6 PL intensity enhancement in perovskite films for n = 10. (a) Absorbance spectra of Ag NPs deposited on glass substrate at different sputtering powers (vertical black line at 532 nm). (b) Normalized PL intensity of the perovskite films without Ag (black line) and with a Ag NPs deposited at sputtering powers of 47 W, 55 W, 110 W, and 120 W.

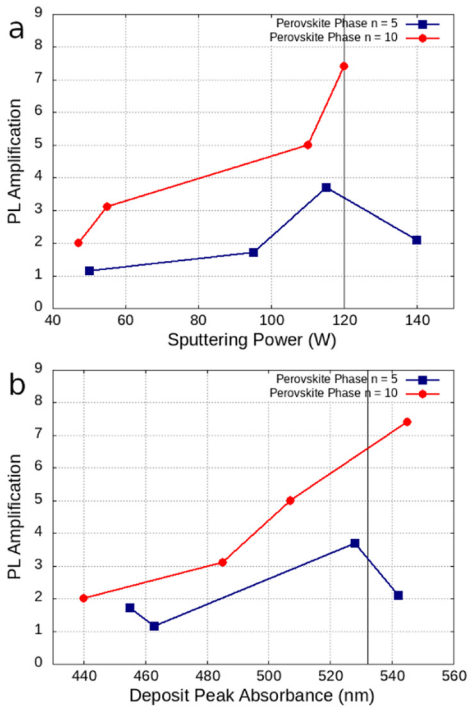

Fig. 7 PL amplification of perovskite films for phase n = 5 and n = 10 (a) PL amplification as a function of sputtering power, with a reference black line at 120 W. (b) PL amplification as a function of the peak absorbance of Ag NPs deposits, with a reference black line at 532 nm.

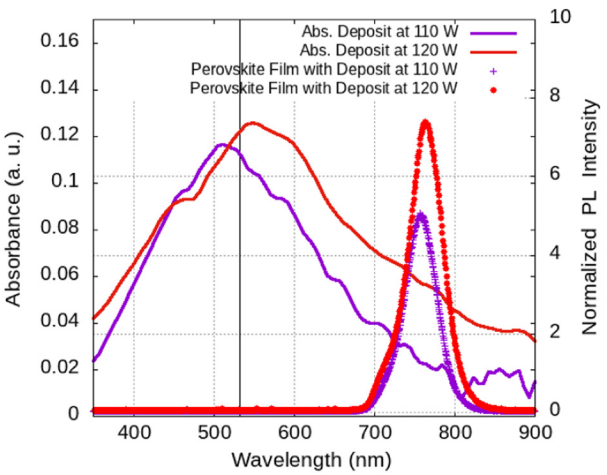

Fig. 8 Comparison of PL amplification for different Ag NPs deposit with similar absorbance spectra. Ag nanoparticle (NP) coatings prepared using sputtering powers of 110 W and 120 W produced similar absorbance spectra on a glass substrate. However, when applied to $(PEA)_2(MA)_9Pb_{10}I_{31}$ (n = 10) perovskite films, these coatings resulted in different PL amplification.

combination of ellipsoidal and amorphous Ag NPs. In comparison, the deposit at 110 W yielded a combination of both ellipsoidal and amorphous Ag NPs. This variation in morphology influenced the LSP resonance. Morphological deformations in the Ag NPs modified the LSP wavelength, leading to variations in plasmonic excitation when exposed to the 532 nm laser beam, thereby limiting PL amplification. In contrast, Ag NPs with well-defined shapes enabled stronger plasmon resonances that more closely matched the excitation wavelength. This alignment facilitated a more uniform near-field interaction with the perovskite sub-layers, resulting in enhanced PL amplification. Fig. 9 schematically illustrates the interaction of the plasmonic electric field with different alignments of perovskite sub-layers.

The energy transfer equation plays a key role in determining the distance between the perovskite molecules and Ag NPs. The energy transfer is given by the interaction potential between the donor dipole (μ_D) and acceptor dipole (μ_A) by

$$V_{DA} = \frac{k}{4\pi\varepsilon_0}\frac{\mu_D\mu_A}{R^3} \quad (1)$$

where R is the distance between them, with the Ag NPs donor and acceptor perovskite sub-layers (Fig. 10). In this way, the hot electron injection between the Ag NPs and perovskite sub-layers is reduced by the spacing generated by the PEA by a factor of R^3 (Fig. 9). However, energy transfer is proportional to the dipole moment, representing the LSP resonance. Thus, both the shape and size of the NPs and the perovskite phase play crucial roles in hot electron transfer under the excitation source.

However, perovskite films with a phase of n = 3 did not exhibit an increase in PL intensity; instead, they showed a quenching effect. This outcome is supported by two arguments associated to the characteristics of low-phase $(PEA)_2(MA)_{n-1}Pb_nI_{3n+1}$

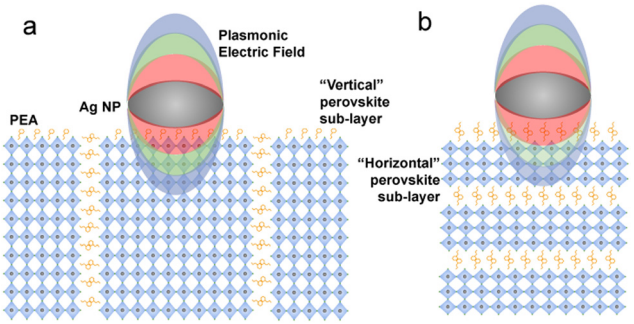

Fig. 9 Illustration of the interaction volume between perovskite sub-layers and the plasmonic electric field of NPs. The electric field generated by the LSP interacts with a larger number of perovskite molecules as the perovskite phase increases, due to alignment and thickness of the sub-layer. (a) "Vertical" and (b) "horizontal" alignment of perovskite sub-layers.

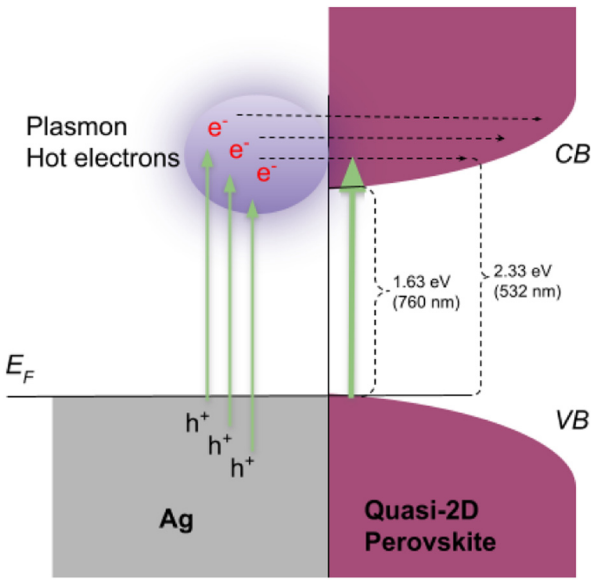

Fig. 10 Schematic representation of hot electrons injection from Ag NPs into the conduction band of perovskite film. Hot electrons are generated in Ag NPs through LSP resonance when excited by the laser source. These electrons move to high-energy states as "hot electrons". Once their energy surpasses 1.63 eV (the perovskite PL peak), they are injected into the high-energy conduction bands of the perovskite film.

perovskites. In the study conducted by Mingjian Yuan (2016),[12] the band-gaps for different perovskite phases are presented, revealing a significant difference between the n = 3 and n = 5 phases. Although both quasi-2D perovskites exhibit the same valence band maximum at −5.27 eV, the n = 3 phase has a conduction band minimum at −3.17 eV, in contrast to the −3.55 eV conduction band minimum of the n = 5 phase. This 0.38 eV difference in the band-gap is critical, as it creates an energy barrier that prevents hot electrons from the plasmons from being injected into the conduction band of the n = 3 phase and blocking PL amplification. Additionally, it has been established that low-phase (n = 1–4) perovskites exhibit a "horizontal" alignment and a higher concentration of PEA, in contrast to their high-phase (n = 5–10) counterparts, which display a "vertical" alignment.[34] The spacing between the PEA and sub-layers reduces the number of perovskite molecules interacting with the plasmonic electric field generated by the Ag NPs. Thus, vertically aligned sub-layers interact with a larger volume of perovskite molecules in the LSP field (see Fig. 9). These findings, along with the results presented in Fig. 4 indicate that the PL enhancement by Ag NPs is not optimal for low-phase (n = 1–4) of $(PEA)_2(MA)_{n-1}Pb_nI_{3n+1}$ perovskites. This finding also helps to explain why a PL blueshift is observed as n increases since, as shown in Fig. 9, the compaction of the perovskite increases with n for the phases analyzed in this work, strengthening the confinement effect.

This study provides indirect evidence for the orientation of the inner sub-layers in quasi-2D perovskites. When the sub-layers are horizontally oriented, the phenethylammonium acts as a separator and insulator, as previously discussed by Ortiz-Cervantes *et al.* (2019).[11] Under these conditions, the insulating layer blocks high-energy electrons generated by plasmonic electric interactions in low-phase perovskite films. In contrast, in vertically oriented sub-layers with a high phase value, the electrons can flow efficiently along the perovskite structure. For this reason, the orientation of the sub-layers in quasi-2D perovskite films has been a subject of significant interest in recent years, with studies demonstrating improved optical and electrical properties in high n-phase perovskites, as reported by H. Tsai *et al.* (2016)[35] and R. Quintero-Bermudez *et al.* (2018).[34] However, as the phase-number increases, the range of synthesized n-phases broadens within the sample. For instance, a perovskite film recipe designed for n = 10 may include sub-layers with n values ranging from 5 to 10. Despite this variation, all sub-layers consistently maintain a vertical orientation, ensuring enhanced properties across the entire film.

Finally, a spectrofluorometer (Edinburgh Instruments FS5) was used to investigate the influence of Ag deposition on the excitation spectrum of quasi-2D perovskite films. The study was carried out covering the extension of the samples surface, with excitation wavelengths ranging from 400 nm to 600 nm, while monitoring emissions at the maximum PL wavelength of 770 nm. Fig. 11 presents the excitation spectrum of a perovskite film with n = 10 before Ag deposition (black curve), exhibiting a peak PL emission when excited at 448 nm. This emission decreases significantly when exciting beyond 500 nm, particularly at 532 nm, which corresponds to the excitation laser wavelength previously used to measure the plasmonic enhancement. The deposition of an Ag coating at a sputtering power of 40 W induced significant spectral modifications: while the excitation peak near 450 nm remained, its intensity decreased and a new peak emerged when exciting at 517 nm. A perovskite film coated at 107 W (blue curve) exhibited further PL enhancement when stimulating beyond 500 nm wavelength, with an excitation peak at 520 nm. Finally, a perovskite film coated at 114 W displayed maximum PL emission when excited at 521 nm.

These findings confirm that Ag deposition induces substantial modifications in the excitation mechanism of perovskite

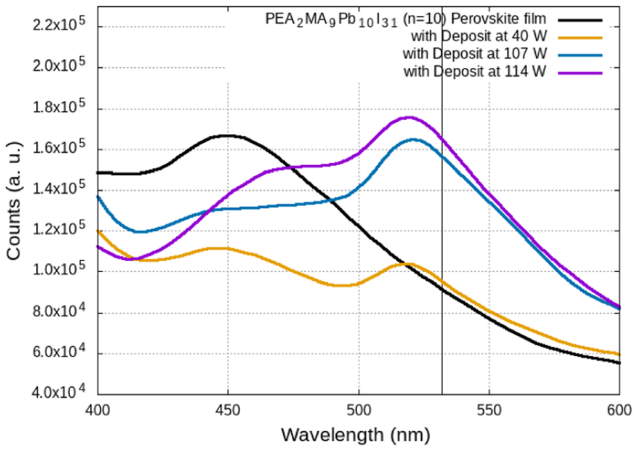

Fig. 11 Excitation spectrum of perovskite films of $(PEA)_2(MA)_9Pb_{10}I_{31}$ (n = 10). Excitation spectra of a perovskite film without Ag NPs (black curve) and perovskite films with Ag deposited at sputtering powers of 40 W (yellow), 107 W (blue), and 114 W (purple) (black line at 532 nm).

films, enhancing the generation of electron–hole pairs when exciting within the spectral range corresponding to the Suns peak emission or, in our case, when exciting with a laser wavelength of 532 nm. The observed increase in PL is attributed to the generation of highly energetic electron–hole pairs and their subsequent recombination.[36] In photovoltaic applications, these energetic charge carriers can be efficiently redirected by the electron transport layer (ETL) and hole transport layer (HTL), thereby enhancing current generation. Rather than simply increasing photoluminescence, this redistribution of charge carriers could improve the efficiency of solar energy conversion. Therefore, Ag NPs coatings on quasi-2D perovskite films represent a promising approach to optimize their optoelectronic properties and enhance the performance of solar cells.

4. Summary and conclusions

We have demonstrated that depositing Ag NPs *via* sputtering on quasi-2D $(PEA)_2(MA)_{n-1}Pb_nI_{3n+1}$ perovskites is an effective and accessible method for enhancing the PL of these advanced materials. The Ag NPs coatings were simultaneously applied to the perovskite films, glass substrates, and TEM grids, enabling a comprehensive study of their effects on the optical properties of the perovskites and the characterization of the Ag NP coatings. Therefore, PL measurements conducted on the perovskite films both before and after Ag NPs deposition revealed significant enhancement in the PL for phases n = 5 and n = 10. These results are directly related to the lower energy bandgap exhibited by these phases compared to lower phases, such as n = 3. Consequently, hot electrons generated using a 532 nm laser beam were sufficiently energetic to be efficiently injected into the conduction band of the n = 5 and n = 10 phases.

Optimal matching between the plasmonic resonance in the Ag NPs and the excitation source, as well as with the morphology of the Ag NPs, emerged as key factors influencing PL enhancement. For the n = 5 phase, the maximum PL amplification observed was a 3.7-fold increase with deposits generated at a sputtering power of 115 W. These deposits exhibited an absorbance peak at 528 nm (measured on glass substrates) and an Ag NP size distribution centered at 8 nm (±0.2 nm), when excited with a 532 nm wavelength laser. For the n = 10 phase, the maximum PL amplification measured was a 7.4-fold increase with a deposit generated at a sputtering power of 120 W. These deposits showed an absorbance peak at 545 nm and a Ag NPs size distribution centered at 7.5 nm (±0.2 nm). Notably, deposits generated at 115 W and 120 W sputtering powers exhibited spherical and ellipsoidal shapes, which enhanced plasmonic resonance and maximized PL amplification in the different perovskite phases.

This study highlights the significant influence of Ag NPs on the optical response of quasi-2D perovskite films, suggesting their potential to improve light-emitting and photovoltaic devices through plasmonic nanostructure engineering strategies. The injection of hot carriers from plasmonic NPs into the band structure of perovskites to amplify PL can be extended to exciton generation in semiconductors, enhancing different optoelectronic effects and applications.

Author contributions

Emmanuel delaCruz-Pina: conceptualization, methodology, investigation, data curation, formal analysis, writing – original draft. Carina Pareja-Rivera: methodology, writing – original draft. Dulce Zugasti-Fernandez: methodology. Arturo Rodriguez-Gomez: methodology, supervision, writing – review and editing. Diego Solis-Ibarra: supervision, writing – review and editing. Jorge Alejandro Reyes-Esqueda: conceptualization, data curation, formal analysis, supervision, validation, writing – review and editing, funding acquisition, project administration.

Data availability

The data supporting this article are included in the ESI.†

Conflicts of interest

The authors declare that they have NO affiliations with or involvement in any organization or entity with any financial interest in the subject matter or materials discussed in this manuscript.

Acknowledgements

E. d-P. thanks CONAHCyT for PhD fellowship. Additionally, we acknowledge the financial support provided by the "PROGRAMA DE BECAS DEL INSTITUTO DE FÍSICA (PBIF24)", UNAM. This research was partially funded by the ECOS-Nord CONAHCyT-ANUIES 315658, PAPIIT-UNAM IN112022, PAPIIT-UNAM IG100825 and PAPIIT-UNAM IN109122. J.A.R.E. is grateful for the sabbatical funding from PASPA-DGAPA-UNAM, CONAHCyT, and the University of Sherbrooke. The authors

acknowledge the technical assistance provided by Gerardo Daniel Rayo López from IF-UNAM. Additionally, they extend their gratitude to Roberto Hernández Reyes and Diego Armando Quiterio Vargas from LCM-IFUNAM for providing the TEM images.

References

1 B. R. Sutherland and E. H. Sargent, *Nat. Photonics*, 2016, **10**, 295–302.
2 K. Lin, J. Xing, L. N. Quan, F. P. G. de Arquer, X. Gong, J. Lu, L. Xie, W. Zhao, D. Zhang and C. Yan, *et al.*, *Nature*, 2018, **562**, 245–248.
3 S. Maiti, M. van der Laan, D. Poonia, P. Schall, S. Kinge and L. D. Siebbeles, *Chem. Phys. Rev.*, 2020, **1**, 011302.
4 H. J. Snaith, *Nat. Mater.*, 2018, **17**, 372–376.
5 Q. Zhang, R. Su, W. Du, X. Liu, L. Zhao, S. T. Ha and Q. Xiong, *Small Methods*, 2017, **1**, 163–170.
6 J. Y. Kim, J.-W. Lee, H. S. Jung, H. Shin and N.-G. Park, *Chem. Rev.*, 2020, **120**, 7867–7918.
7 S. Pierini, M. dAmato, M. Goyal, Q. Glorieux, E. Giacobino, E. Lhuillier, C. Couteau and A. Bramati, *ACS Photonics*, 2020, **7**, 2265–2272.
8 H. Utzat, W. Sun, A. E. Kaplan, F. Krieg, M. Ginterseder, B. Spokoyny, N. D. Klein, K. E. Shulenberger, C. F. Perkinson and M. V. Kovalenko, *et al.*, *Science*, 2019, **363**, 1068–1072.
9 Y.-S. Park, S. Guo, N. S. Makarov and V. I. Klimov, *ACS Nano*, 2015, **9**, 10386–10393.
10 A. K. Jena, A. Kulkarni and T. Miyasaka, *Chem. Rev.*, 2019, **119**, 3036–3103.
11 C. Ortiz-Cervantes, P. Carmona-Monroy and D. Solis-Ibarra, *ChemSusChem*, 2019, **12**, 1560–1575.
12 M. Yuan, L. N. Quan, R. Comin, G. Walters, R. Sabatini, O. Voznyy, S. Hoogland, Y. Zhao, E. M. Beauregard and P. Kanjanaboos, *et al.*, *Nat. Nanotechnol.*, 2016, **11**, 872–877.
13 I. C. Smith, E. T. Hoke, D. Solis-Ibarra, M. D. McGehee and H. I. Karunadasa, *Angew. Chem., Int. Ed.*, 2014, **53**, 11232–11235.
14 S. I. Azzam, A. V. Kildishev, R.-M. Ma, C.-Z. Ning, R. Oulton, V. M. Shalaev, M. I. Stockman, J.-L. Xu and X. Zhang, *Light: Sci. Appl.*, 2020, **9**, 90.
15 R. F. Oulton, V. J. Sorger, D. Genov, D. Pile and X. Zhang, *Nat. Photonics*, 2008, **2**, 496–500.
16 C. Cirac, R. Jurga, M. Khalid and F. Della Sala, *Nanophotonics*, 2019, **8**, 1821–1833.
17 V. Amendola, R. Pilot, M. Frasconi, O. M. Maragò and M. A. Iat, *J. Phys.: Condens. Matter*, 2017, **29**, 203002.
18 M. Li, S. K. Cushing and N. Wu, *Analyst*, 2015, **140**, 386–406.
19 C. Huang, W. Sun, Y. Fan, Y. Wang, Y. Gao, N. Zhang, K. Wang, S. Liu, S. Wang and S. Xiao, *et al.*, *ACS Nano*, 2018, **12**, 3865–3874.
20 N. Deka, M. Islam, P. K. Sarswat and G. Kumar, *Vacuum*, 2018, **152**, 285–290.
21 M. Notarianni, K. Vernon, A. Chou, M. Aljada, J. Liu and N. Motta, *Sol. Energy*, 2014, **106**, 23–37.
22 N. Liu, M. Mesch, T. Weiss, M. Hentschel and H. Giessen, *Nano Lett.*, 2010, **10**, 2342–2348.
23 L. Gu, K. Wen, Q. Peng, W. Huang and J. Wang, *Small*, 2020, **16**, 2001861.
24 O. Bitton and G. Haran, *Acc. Chem. Res.*, 2022, **55**, 1659–1668.
25 Z. Li, Y. Xiao, Y. Gong, Z. Wang, Y. Kang, S. Zu, P. M. Ajayan, P. Nordlander and Z. Fang, *ACS Nano*, 2015, **9**, 10158–10164.
26 S. E. Guerrero, R. Nava and J.-A. Reyes-Esqueda, *J. Lumin.*, 2024, **269**, 120465.
27 J. Dong, W. Gao, Q. Han, Y. Wang, J. Qi, X. Yan and M. Sun, *Rev. Phys.*, 2019, **4**, 100026.
28 J. B. Khurgin, *Nanophotonics*, 2020, **9**, 453–471.
29 J.-E. Park, J. Kim and J.-M. Nam, *Chem. Sci.*, 2017, **8**, 4696–4704.
30 S. Kasani, K. Curtin and N. Wu, *Nanophotonics*, 2019, **8**, 2065–2089.
31 B. Ai, Z. Fan and Z. J. Wong, *Microsyst. Nanoeng.*, 2022, **8**, 5.
32 R. Siavash Moakhar, S. Gholipour, S. Masudy-Panah, A. Seza, A. Mehdikhani, N. Riahi-Noori, S. Tafazoli, N. Timasi, Y.-F. Lim and M. Saliba, *Adv. Sci.*, 2020, **7**, 1902448.
33 Q. Luo, C. Zhang, X. Deng, H. Zhu, Z. Li, Z. Wang, X. C hen and S. Huang, *ACS Appl. Mater. Interfaces*, 2017, **9**, 34821–34832.
34 R. Quintero-Bermudez, A. Gold-Parker, A. H. Proppe, R. Munir, Z. Yang, S. O. Kelley, A. Amassian, M. F. Toney and E. H. Sargent, *Nat. Mater.*, 2018, **17**, 900–907.
35 H. Tsai, W. Nie, J.-C. Blancon, C. C. Stoumpos, R. Asadpour, B. Harutyunyan, A. J. Neukirch, R. Verduzco, J. J. Crochet and S. Tretiak, *et al.*, *Nature*, 2016, **536**, 312–316.
36 I. Ahmed, L. Shi, H. Pasanen, P. Vivo, P. Maity, M. Hatamvand and Y. Zhan, *Light: Sci. Appl.*, 2021, **10**, 174.